Reversible pH-controlled DNA-binding peptide nanotweezers: An in-silico study

Gaurav Sharma[1]
Kaushal Rege[2,3]
David E Budil[4]
Martin L Yarmush[2,5]
Constantinos Mavroidis[1]

[1]Department of Mechanical and Industrial Engineering; [4]Department of Chemistry and Chemical Biology, Northeastern University, Boston, MA, USA; [2]The Center for Engineering in Medicine (CEM), Massachusetts General Hospital and Harvard Medical School, Boston, MA, USA; [3]Department of Chemical Engineering, Arizona State University, Tempe, AZ, USA; [5]Department of Biomedical Engineering, Rutgers University, NJ, USA

Correspondence: Constantinos Mavroidis Department of Mechanical and Industrial Engineering, 360 Huntington Avenue, Northeastern University, Boston, MA, 02115, USA
Tel +1 617 373 4121
Fax +1 617 373 2921
Email mavro@coe.neu.edu

Abstract: We describe the molecular dynamics (MD)-aided engineering design of mutant peptides based on the α-helical coiled-coil GCN4 leucine zipper peptide (GCN4-p1) in order to obtain environmentally-responsive nanotweezers. The actuation mechanism of the nanotweezers depends on the modification of electrostatic charges on the residues along the length of the coiled coil. Modulating the solution pH between neutral and acidic values results in the reversible movement of helices toward and away from each other and creates a complete closed-open-closed transition cycle between the helices. Our results indicate that the mutants show a reversible opening of up to 15 Å (1.5 nm; approximately 150% of the initial separation) upon pH actuation. Investigation on the physicochemical phenomena that influence conformational properties, structural stability, and reversibility of the coiled-coil peptide-based nanotweezers revealed that a rationale- and design-based approach is needed to engineer stable peptide or macromolecules into stimuli-responsive devices. The efficacy of the mutant that demonstrated the most significant reversible actuation for environmentally responsive modulation of DNA-binding activity was also demonstrated. Our results have significant implications in bioseparations and in the engineering of novel transcription factors.

Keywords: bionanotechnology, nanotweezers, coiled-coil, GCN4, leucine zipper, molecular dynamics, environmentally responsive peptides, transcription factor engineering

Introduction

The development of environmentally-responsive functional 'nanodevices', capable of performing complex tasks at nanoscale, will require the assembly of individual nanoscale components. Most reports in the literature have focused on inorganic nanoparticles including buckyball fullerenes and carbon nanotubes (Tenne 2006), and various metal (Hirsch et al 2006) and semiconductor (Biju et al 2008) nanoparticles. These systems can have significant implications in a variety of applications including molecular electronics, sensors, and drug delivery. In nature, many manipulations at the nanoscale are carried out by proteins and peptides that serve a variety of structural (Bella et al 1994) and mechanical (Lee et al 2006) functions. Therefore, it is of great interest to engineer naturally-occurring peptides and proteins as functional components that can be eventually assembled as novel nanodevices (Banta et al 2007) in combination with other environmentally responsive nanomaterials.

A number of tools are already in place to manipulate the vast repertoire of naturally occurring proteins and peptides. Structural information, obtained by techniques such as X-ray crystallography and nuclear magnetic resonance (NMR), has provided an intricate picture of the conformational attributes of proteins. Coupling this information with data obtained by dynamic molecular simulations (Karplus and McCammon 2002; Tama and Brooks 2006) and nanoscale manipulation (Tinoco and Bustamante 2002; Bao and Suresh 2003; Bustamante 2004) has enabled the correlation of protein structure and function (Mizoue and Chazin 2002; Daggett and Fersht 2003). The breadth of

structure and function in proteins and peptides has been enhanced by protein engineering, which provides the capability to modify existing proteins or generate new ones (Brannigan and Wilkinson 2002; Bloom et al 2005).

Transcription factors are proteins that bind to specific DNA sequences in the promoter and enhancer regions thereby regulating gene transcription. The basic leucine-zipper (bZIP) motif of the yeast transcription factor GCN4 (Ellenberger et al 1992) is a 56-residue peptide (residues 225–281) which consists of two sub-domains: the leucine zipper (GCN4-LZ) dimerization domain and the basic DNA-binding domain (Figure 1a). The leucine zipper region forms a stable, two-stranded, parallel coiled-coil (O'Shea et al 1991) in which individual residues follow a heptad repeat pattern $(a \cdot b \cdot c \cdot d \cdot e \cdot f \cdot g)_n$; residues in the a and d position are primarily hydrophobic, and residues in the e and g position are predominantly charged or polar (Figure 1c). The coiled-coil structure is highly stable largely due the hydrophobic interactions at the interface of the two helices and the complementary electrostatic interactions between individual amino acids that

stabilize the structure as a knobs-in-hole model (Crick 1953). GCN4-LZ consists of two identical 33-residue polypeptide chains/helices and is ~4.5 nm long and ~3 nm wide. The helices wrap around each other to form approximately ¼ turn of a left-handed supercoil. The pitch of the supercoil averages 181 Å, and the average distance between the helix axes is 9.3 Å (O'Shea et al 1991). Figure 1b shows the enlarged view of the leucine zipper with the corresponding dimensions.

Coiled-coil proteins play an important role as transcriptional activators (Barbara et al 2007) and in membrane fusion (Harbury 1998; Weis and Scheller 1998). The simplicity and regularity in their structure make them excellent candidates for protein design and engineering studies. For example, folding pathways in coiled-coil proteins have been studied as model systems for quaternary structure formation in proteins (Mason and Arndt 2004). Coiled-coil motif-based dimers and trimers of α-helices have been designed to act as functional protein receptors for molecular recognition of ligands (Doerr et al 2004) and heterodimerizing leucine zipper coiled-coils have been designed to deliver radionuclides
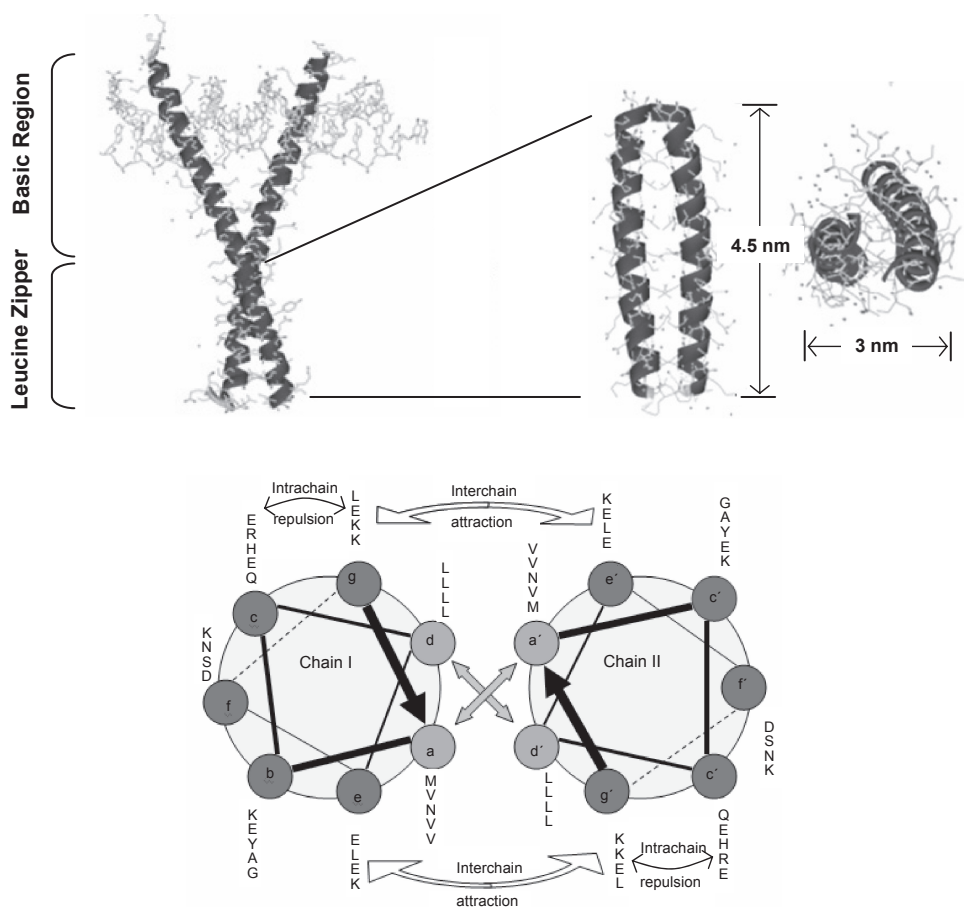

Figure 1 a) Coiled-coil GCN4 bound to DNA showing the basic and the leucine zipper regions; **b)** Enlarged view of the leucine zipper region showing the side (*Left*) and top (*Right*) views and the corresponding dimensions; **c)** Helical wheel diagram of the leucine zipper motif showing the positions of the residues and the interactions stabilizing the coiled-coil motif. Shaded arrows in the middle indicate hydrophobic interactions. Letters indicate residues at each position according to their type.

to the surface of cancer cells (Moll et al 2001). Coiled-coil proteins have been extensively investigated using various experimental techniques such as NMR (Nikolaev and Pervushin 2007), X-ray diffraction (O'Shea et al 1991), circular dichroism (CD) and fluorescence spectroscopy (Suzuki et al 1998), differential scanning calorimetry (DSC) (Yu et al 1996) and electron spin resonance (ESR) spectroscopy (Columbus and Hubbell 2004) as well as theoretical and computational approaches using molecular dynamics (MD) simulation techniques (Mohanty et al 1999; Missimer et al 2005; Pineiro et al 2005). MD simulations provide a means to understand the structural and dynamic behavior of coiled-coil at the atomic level which is often inaccessible to experimental tools.

In the present work, we describe the molecular dynamics-aided design, concept evolution and biophysical characterization of an engineered peptide nanotweezer based on the coiled-coil GCN4-LZ. The simplicity, regularity in structural organization, and availability of the peptide crystal structure allows the engineering of GCN4-LZ to develop functional nanoscale elements. The GCN4-LZ was engineered to obtain pH-dependent nanotweezers involving the lateral displacement of the two helices relative to each other. The reversible actuation mechanism depends on the generation of similar electrostatic charges along the peptide chain which forces the two coils to repel each other, creating a closed-to-open transition. Neutralizing these charges leads to an open-to-closed transition and restitution of the original structure stabilized primarily by hydrophobic interactions. Figure 2a shows a schematic of the nanotweezer operating principle. A broader impact of this study was the analysis of coiled-coil stability under different pH conditions in addition to an in-depth investigation into the effect of point mutations and electrostatic forces on coiled-coil secondary structure. Based on these studies, we propose the design of a DNA-binding modulator element based on the pH-driven nanotweezer architecture and show preliminary simulation results to support our hypothesis. The development of such a DNA-binding modulator has implications in transcription factor engineering wherein one of the focuses is the construction of designer transcription factors for various therapeutic and research applications (Beerli and Barbas 2002). We also describe the development of key design principles required for incorporating flexibility in rigid peptide motifs which can have implications in computational drug design (Carlson and McCammon 2000), design of protein-based biosensors (Gooding et al 2003) and molecular motors (Sun et al 2003).
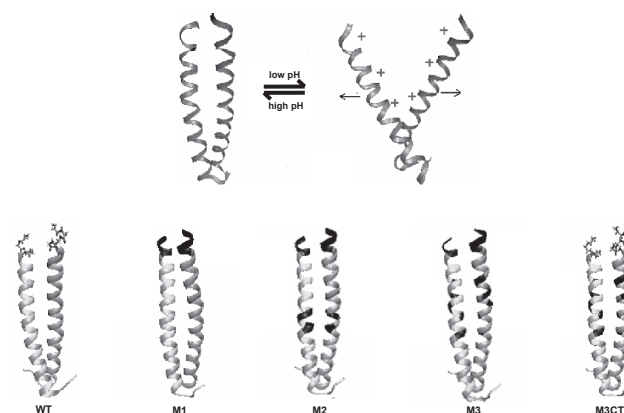

Figure 2 a) Schematic of the operating principle of nanotweezer. Initial 'closed' state at neutral pH (*Left*). Final 'open' state generated at low pH (*Right*). The *plus* signs in the 'open' state represent the location of engineered histidine residues which becomes positively charged at low pH thereby creating electrostatic repulsive forces; **b**) Nanotweezer mutants; Wild-Type (WT), Mutants M1, M2, M3, and the M3 control (M3CT). The position of glycine tag in WT and M3CT is shown in 'bond' representation. Position of His-tags and histidine mutations in other mutants is shown in dark shades.

Methods
Peptide design

The X-ray crystallographic structure of the native GCN4 (PDB entry: 1YSA), complexed with AP-1 yeast DNA, was obtained from the Protein Data Bank (see Figure 1a). The DNA was removed by deleting the coordinates from the PDB structure and the two peptide chains (A and B) were truncated to contain 33 residues numbered 249 to 281 corresponding to the coiled-coil portion of the peptide (henceforth referred to as GCN4-LZ); an arginine residue, missing at position 281 of chain B in the original crystal structure was added. A cysteine residue was also introduced at position 248 in both chains in order to enable interhelical bonding and dimerization.

Three different nanotweezer mutants (M1, M2, and M3) were designed using GCN4-LZ as template. First, a pentaglycine tag was added at the N-terminus of GCN4-LZ; the glycine (Gly) residues were added in order to maintain the same number of residues as those in the nanotweezer mutants described below. The resulting structure is referred to as the wild-type (WT) peptide in subsequent discussions. Mutant M1 consists of a pentahistidine tag (His-tag) aligned with the α-helix at the N-terminus of the wild-type. Mutant M2 consists of four mutations (L261H, S262H, N264H, and Y265H) in each of the two helical chains in addition to the N-terminal His-tags present in M1. Mutant M3 consists of five mutations (L253H, K256H, E259H, L261H, and Y265H) in each of the helical chains in addition to the His-tag. Finally, in mutant M3CT we replaced the His-tag of mutant M3 with a pentaglycine tag. These mutation

sites were chosen based on the MultiCoil (Wolf et al 1997) predictions for the coiled-coil formation probability of each of the mutants; a probability greater than 0.8 was seen for all engineered mutants. Figure S-1 shows the MultiCoil score for the mutants; the probability cut-off for coiled coil formation is 0.5 (Wolf et al 1997). Table 1 shows the single-letter amino acid sequences of the wild-type and the mutant peptides with the residue positions shown against the coiled-coil heptad repeat sequence. Figure 2b shows the architecture of different nanotweezer mutants with the position of His-tags and histidine residues shown.

Molecular dynamics

The protonation states of histidine (His), glutamic acid (Glu), and asparatic acid (Asp) residues were modified appropriately to model neutral and low pH. His residues are unprotonated at neutral pH whereas Glu and Asp are negatively charged. At low pH, His are protonated and therefore, positively charged, whereas Asp and Glu are considered neutral. $N\epsilon2H$ and $N\delta1H + N\epsilon2H(+)$ tautomeric states of His were considered to model neutral and low pH, respectively. For Glu $O\epsilon2(-)$ and $O\epsilon2H$ tautomeric states were considered to model neutral and low pH, respectively. For Asp $O\delta2(-)$ and $O\delta2H$ tatutomeric states were considered to model neutral and low pH, respectively.

The Nanoscale Molecular Dynamics (NAMD) (Phillips et al 2005) program was used to perform MD simulations in this study. The protein was modeled with an all-atom CHARMM27 force field (MacKerell et al 1998). The protein was solvated by placing it at the center of a box of water with approximate edge lengths of $50 \times 50 \times 70$ Å and subtracting all water molecules within 2.4 Å of any protein atom. Water molecules were described by the TIP3P model (Jorgensen 1983). The system being studied carries excess charge at low pH due to the protonation of amino acids in the peptide.

To represent a typical biological environment which is electrically neutral, salt (NaCl, 2 mM) was added by placing ions in water to make the system neutral. Electrostatic interactions were computed using the particle mesh Ewald (PME) method (Darden et al 1993). Van der Waals interactions were truncated at a cutoff distance of 12 Å and a smooth switching function was used at a switching distance of 10 Å. The ShakeH (van Gunsteren and Berendsen 1977) algorithm was used to fix the bond between each hydrogen and its mother atom to the nominal bond length with a relative tolerance of 1.0×10^{-8} Å and the timestep for integration was 2 fs. The temperature was regulated by coupling the system to an external bath with a damping coefficient of 5. An isobaric (P = 1 atm) and isothermal (T = 298 K) with constant number of atoms (the so-called NPT) ensemble was created using the approach developed by Nose and Hoover (Martyna et al 1994).

Each MD simulation consisted of four individual steps. In the first, the system was minimized for 2000 steps using the conjugate gradient method with the protein fixed in space. This allowed the water to relax and absorb around the protein. The constraints on the protein were then removed in the second step and the entire system was minimized for 2000 steps. In the third step, the system was heated to the desired temperature within 10 ps and then allowed to equilibrate for another 10 ps at the target temperature with the protein constrained through a harmonic potential. The constraints were then removed and the system was allowed to evolve for 4–5 ns of production run. The trajectory was saved every 2 ps. The evolution of the secondary structure during MD trajectories was calculated using the STRIDE (Frishman and Argos 1995) program.

MD methods for DNA-binding simulation

Steered Molecular Dynamics (SMD) (Isralewitz et al 2001) technique was used for DNA-binding modulation

Table I Naming convention and residue sequence for nanotweezer mutants. The top row shows the haptad repeat sequence of a coiled-coil protein. In the bottom rows the residue sequence of individual mutants is arranged in group of seven to highlight their consensus with the coiled-coil heptad repeat pattern.

Mutant name	Sequence				
Coiled-coil		a b c d e f g	a b c d e f g	a b c d e f g	a b c d e f g
WT	[243]GGGGGCR	MKQLEDK	VEELLSK	NYHLENE	VARLKKL	VGER[281]
M1	HHHHHCR	MKQLEDK	VEELLSK	NYHLENE	VARLKKL	VGER
M2	HHHHHCR	MKQLEDK	VEELHHK	HHHLENE	VARLKKL	VGER
M3	HHHHHCR	MKQHEDH	VEHLHSK	NHHLENE	VARLKKL	VGER
M3CT	GGGGGCR	MKQHEDH	VEHLHSK	NHHLENE	VARLKKL	VGER

simulation. This technique has been used extensively to study the mechanical properties of proteins and biopolymers (Lu and Schulten 1999; Cheng et al 2002; Gao et al 2002; Lu and Long 2005). The DNA molecule was pulled out of the protein-binding site using a constant velocity SMD simulation in which a constant velocity is imparted to the DNA atoms in a predefined direction. This is done by attaching the center-of-mass (COM) of DNA atoms (called SMD atom) to a dummy atom and pulling the dummy atom with a virtual spring of known stiffness. This dummy atom is moved at constant velocity and then the force between both is measured using:

$$F = -\nabla U \quad U = \frac{1}{2} k \left[vt - (r - r_0) \cdot n \right]^2 \qquad (1)$$

where U is the potential energy, k is spring constant, v is the pulling velocity, t is time, r is the actual position of the pulling atom, r_0 is the initial position of the pulling atom, and n is the pulling direction. A harmonic spring of stiffness, $k = 0.2$ kcal/mol/Å^2, was used and the DNA molecule was

pulled along the longitudinal axis of the GCN4 peptide with a constant velocity $v = 10$ Å/ns (Figure 3). At low pH, the N$_1$ atom of A nucleoside (pK$_a$~3.8) and N$_3$ atom of C nucleoside (pK$_a$~4.5) are know to accept a proton, thereby neutralizing the charge on the entire nucleotide (Saenger 1984). At moderate pH (3–5) range only a fraction of the A and C nucleosides can be expected to be protonated. We therefore chose to protonate all of A nucleosides which could effectively correspond to a simulation carried out at pH 4 (Heng et al 2006). Partial charges for the N$_1$-protonated A nucleoside were used as reported in (Heng et al 2006) and were kindly provided by Dr. Aleksei Aksimentiev. The entire GCN4–DNA system was solvated in a water box and neutralized using NaCl salt at 20 mM concentration. All the other simulation parameters are the same as described previously.

Results and discussion

We designed GCN4-LZ mutants with His residues at different positions in the peptide sequence in order to enable
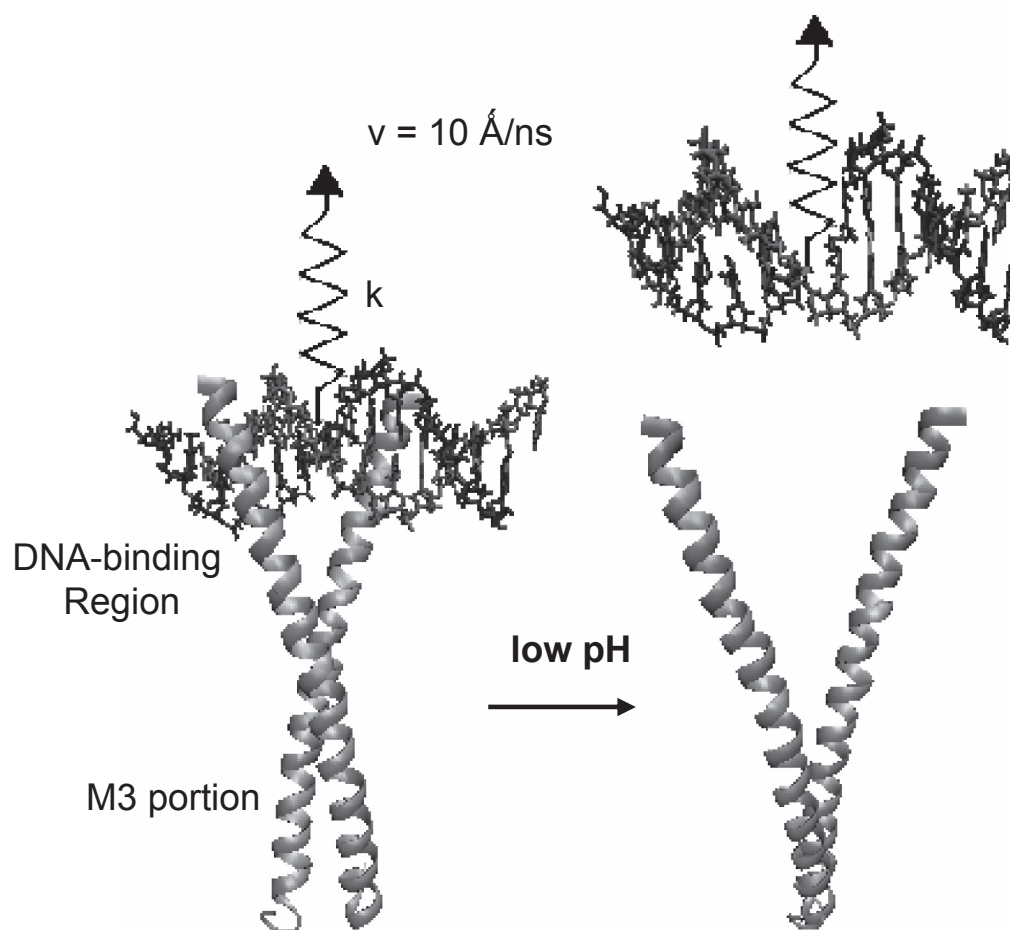

Figure 3 System for studying the DNA-binding modulation of the molecular nanotweezer.

the pH-dependent actuation mechanism. At neutral pH, His residues (histidine pKa ~6.1) are unprotonated and the coiled-coil peptide maintains a 'closed' structure. At low pH, interhelical repulsion induced by His protonation results in the actuation motion of the two helices of the peptide away from each other.

Wild-type structure and mutant M1 are stable

From previous experimental (Kohn et al 1995; Yu et al 1996; Hendsch and Tidor 1999) and computational studies (Mohanty et al 1999; Missimer et al 2005; Pineiro et al 2005), we expect that the wild-type GCN4-LZ will be stable at both neutral and low pH. To address this, we performed simulations starting with the GCN4-LZ crystal structure immersed in a box of water molecules. The backbone Cα root mean square deviation (RMSD) for residues 248–281 does indeed remain low (1.5 Å) over the course of simulation at both neutral and low pH (Figure S-2a). This value agrees well with the previously reported range of RMSD values from MD simulations (Vieth et al 1994; Mohanty et al 1999) of GCN4-LZ. These results are expected since the presence of at least six sites of strong hydrophobic interactions along the helical chain makes the WT peptide highly stable and resistant to any pH perturbation (Figure S-2b). Previous reports in the literature (Kohn et al 1995) also indicate that the GCN4-LZ is stable under conditions of low pH due to the stabilization by increased hydrophobicity of the unionized glutamic acid residues compared to the ionized glutamic acid side-chain at neutral pH. Our results on the stability of GCN4-LZ under acidic pH are in agreement with these studies.

The pH-dependent actuation of mutant M1, which contains a 5-histidine tag at the N-terminus of each helical chain (Figure 2b), was evaluated at both neutral and low pH. It was hypothesized that the protonation of histidine residues in the N-terminal tags at low pH would result in significant electrostatic repulsive forces and 'push' the two helices apart, thus generating the closed-to-open mechanochemical actuation in the mutant peptide. Two atoms (Cα atoms of the His247 residues) were selected near the N-terminal of the individual chains in order to measure the opening between the helices and the distance between the two was measured as a function of simulation time. No significant opening was observed after a 4 ns simulation; the initial distance of 13 Å between the two atoms remained constant during the first nanosecond of simulation after which it increased to 16 Å and remained stable at this separation for the rest of the simulation. The increase of 3 Å is not significant and can be attributed to atomic fluctuations

or the perturbation in the histidine residues due to repulsive forces rather than the overall displacement of the two chains. This implies that the electrostatic repulsive forces generated by the positively charged N-terminal histidines are not sufficient to overcome the strong hydrophobic interactions that stabilize the coiled-coil core of M1 mutant. In order to offset the attractive hydrophobic interactions in the core, we designed subsequent mutants that possess histidine residues along the length of coiled-coil.

Additional repulsive forces are needed to trigger a conformational change in the coiled-coil

Mutant M2 (Figure 2b) was designed next with four histidine residues incorporated within the helical chains in addition to the N-terminal histidine-tag. It was hypothesized that the presence of these additional histidine residues will create a second region of repulsive forces along the interface of the two helices at low pH and trigger conformational displacement between the helices.

Figure 4a shows the snapshots of a 4 ns simulation of M2 at low pH. Mutant M2 was not stable during the course of
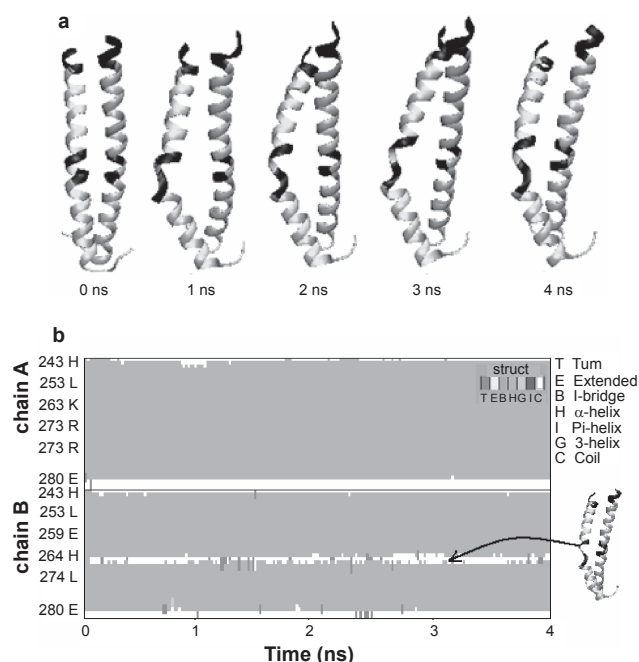

Figure 4 a) Snapshots of a 4 ns simulation of mutant M2 at various time instances. The position of histidine residues are shown in dark shades. The α-helical structure in chain B was disrupted during the simulation implying that some of the mutations are inherently destabilizing for its secondary structure; **b)** Evolution of the secondary structure elements of M2 as a function of time. The coloring scheme is indicated at the top right. The upper and lower halves corresponds to chain A and B respectively while the Y-axis denotes the residue number. The early disruption of the α-helical structure in chain B is evident from the figure.

the simulation as indicated by the disruption of the α-helix in chain B. Moreover, no significant opening was observed in the mutant, implying that either the electrostatic forces were not sufficient or the mutation sites were not well-selected. To gain further insight into the stability of the structure we plotted the evolution of the secondary structure elements of M2 over the simulation time (Figure 4b). Unfolding of the α-helix begins during the first nanosecond of the simulation itself, implying that these mutations were inherently destabilizing to the secondary structure. One explanation for the unfolding of the α-helix lies in the nature of the N264H mutation. The location of the two asparagines (Asn264A and Asn264B) is unique in that they are the only polar residues in the core positions (*a* and *d*) of the GCN4-LZ. The Asn264A–Asn264B interhelical interaction is the strongest favorable interaction between individual groups in the GCN4-LZ and stabilizes the coiled-coil structure by contributing −2.1 kcal/mole towards the free energy of the structure (Hendsch and Tidor 1999). This strong interaction arises from the fact that the two Asn residues

are buried and packed in the 'knobs-into-holes' pattern described by Crick (1953). The N264H mutation replaces this stabilizing interaction of Asn residues with the destabilizing ionic repulsions of the charged His residues thereby disrupting the coiled-coil structure. The resulting structural instability obviates the use of M2 as a potential design since maintaining structural rigidity during the course of operation is an important design requirement for the nanotweezer.

Evolved design of the coiled-coil nanotweezer (mutant M3): Low pH triggers the actuation motion while maintaining the structural integrity

Mutant M3 was designed next with the following point mutations in addition to the N-terminal histidine tag: L253H, K256H, E259H, L261H, Y265H. These mutation sites correspond to the *d*, *g*, *c*, *e*, and *b* positions respectively on the helical wheel diagram (Figure 1c). Figure 5a shows the starting
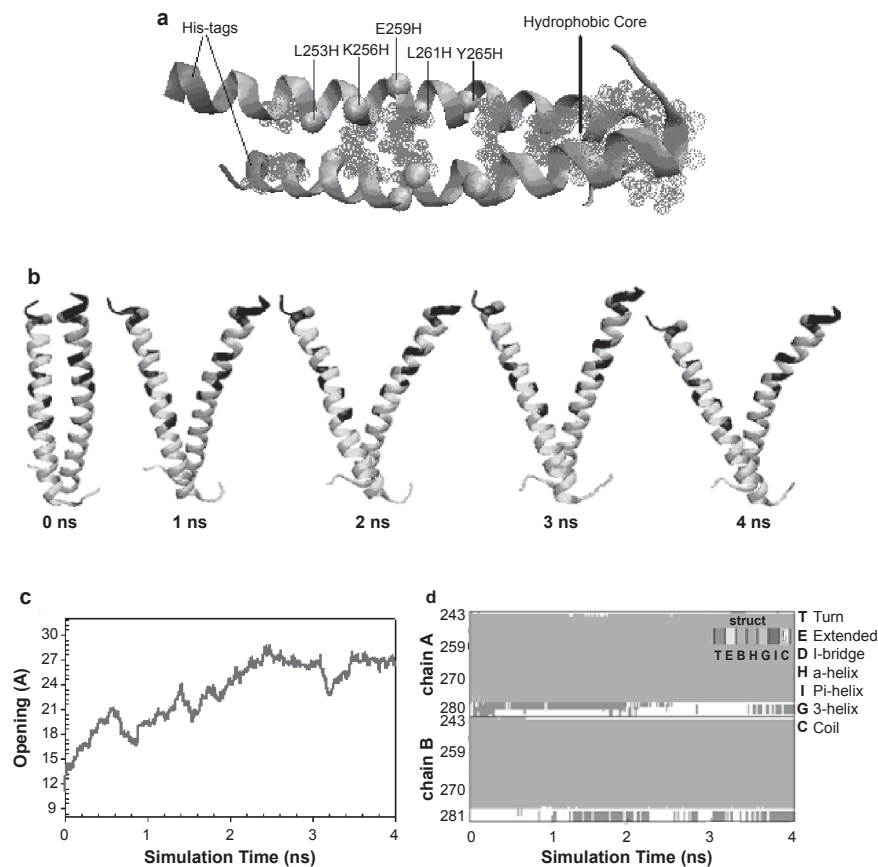

Figure 5 a) Structural details of the M3 mutant. The position of histidine mutations are shown as spheres. Hydrophobic interactions are shown as gray dotted spheres. Note the strong hydrophobic core in the lower half of the protein which serves as a 'hinge' for the nanotweezer design; **b**) Snapshots of mutant M3 at various time instances during a 4 ns simulation. Location of the His246 residue between which the opening is measured is shown as a sphere; **c**) Opening dynamics of M3 at low pH. The initial separation between the two chains was 11 Å which gradually increased to 27 Å at the 2.5 ns stage and then stabilized for the rest of the simulation giving a net opening of 16 Å; **d**) Evolution of the secondary structure elements of M3 mutant as a function of time. The structural features of the two chains were conserved throughout the simulation.

structure of M3 with the His mutation sites shown as spheres. M3 has a uniform distribution of His residues along the helical chain which results in a spatial distribution of electrostatic charges in addition to the concentrated charges from the distal His-tags. Further, the L253H, L261H, and Y265H mutations replace the hydrophobic leucine and tyrosine residues with polar His residues thereby significantly reducing the strength of the hydrophobic interactions towards the N-terminal and 'middle' regions of the coiled-coil core while maintaining the strong hydrophobic core in the C-terminal region. This evolved design was therefore a balance between repulsive forces that can induce the actuation mechanism at low pH and strong hydrophobic interactions that can (i) maintain the coiled-coil structure and (ii) serve as the restoring force for the 'hinge' action in order to restore the original conformation of the peptide at neutral pH. We verified, as predicted from its MultiCoil score (Wolf et al 1997), that these mutations do not destabilize the coiled-coil formation propensity of the individual helices. Interestingly, of all the mutants evaluated, M3 demonstrated the highest probability (0.9) of dimer formation in solution (Figure S-1).

Figure 5b shows the snapshots of a 4 ns simulation of M3. Large conformational changes were observed in the M3 system leading to a significant net opening between the two helices. The helices rapidly moved apart within the first nanosecond and continued to move apart steadily until three nanoseconds (ns) before adopting a final stable conformation. The distance between the Cα atoms of the His246 residues in both chains was plotted as a function of the simulation time (Figure 5c). The initial distance between the two atoms was 11 Å which gradually increased to 28 Å at the 2.5 ns stage. The distance then fluctuated due to the dynamic nature of the electrostatic forces but stayed near the 27 Å separation during the rest of the simulation (4 ns). Thus, a net opening of 16 Å which is approximately 150% of the initial separation (11 Å) was observed for M3 at low pH.

We plotted the evolution of the secondary structure of the simulated system to characterize the effects of electrostatic forces on the structural stability of M3 (Figure 5d). The main structural features of mutant are largely retained, ie, the α-helices of the two chains are preserved throughout the simulation. The last three residues at the C-terminal in both chains remain in their native random coil conformation throughout the simulation and do not affect the stability of the overall structure. This result, in conjunction with the MultiCoil (Wolf et al 1997) prediction (Figure S-1), verifies the hypothesis that selective mutations can be performed in the native GCN4-LZ, inducing large conformational

changes without compromising its structural stability. The conformational change is, however, not uniform along the length of the α-helical chains as is evident from the helix–helix contact map (Figure S-3). The closed-to-open conformational change in M3 results in a loss of helix–helix contacts in residues 243–261 while contacts are largely preserved in residues 262–281. The α-helices appear to 'bend' near the His-261 region as a result of the electrostatic forces. The bending, while maintaining the overall secondary structure, creates elastic forces in α-helices (Seungho and Sean 2005) which tend to bring the helices back to their initial 'relaxed' structure. Thus the 'open' conformation of mutant M3 at low pH is in a state of dynamic equilibrium between the electrostatic repulsive forces from charged residues and the restituting forces created by helix elasticity and coiled-coil hydrophobic interactions.

In order to gain insights into the mechanisms of action of M3, we designed a control mutant, M3CT, by replacing the N-terminal histidines in M3 by an equivalent number of glycine residues. This design enables an investigation into the contribution of the five histidine residues within the coiled-coil core towards the conformational dynamics of the resulting GCN4-LZ mutant, without additional contributions from the distal His-tags. Glycine was chosen since it is a neutral, α-helix breaking amino acid (Aurora et al 1994) and therefore, has no secondary structural or charge contributions to the resulting M3CT mutant. Figure 6 compares the actuation dynamics of all five mutants plotted against time. Mutant M3 shows the most significant actuation followed by the M3CT mutant, further reinforcing the observation that while the N-terminal His-tag contributes towards the actuation, the His mutations
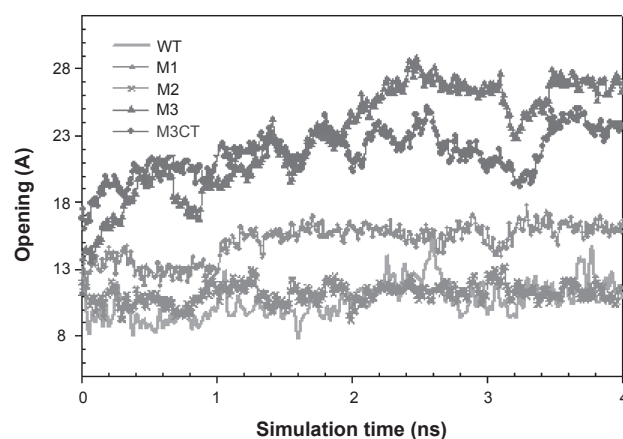

Figure 6 Comparison of opening dynamics for various mutants at low pH. M3 showed the maximum opening of 1.6 nm during the simulation time. The control mutant M3CT initially followed a similar dynamics but lags the net opening of M3 by 0.4 nm. The dynamics of wild-type (WT) and mutants M1, M2 are explained previously.

in the parent GCN4-LZ structure play the critical role. These results are consistent with the lack of closed-to-open transition for M1. The WT and M2 mutants did not show any transition during the simulation as discussed earlier.

Mutant M3 demonstrates reversible pH-dependent actuation

One of the key design goals of a nanotweezer is reversibility of mechanochemical actuation. We therefore investigated whether the mutant M3 demonstrated a reversible open-to-closed transition when the pH reverts back to neutral from acidic. The initial structure (the 'open' state) for this simulation was taken from the final conformation generated from the previous 4-ns closed-to-open simulation at low pH. Histidine, glutamic acid, and aspartic acid residues in M3 were unprotonated to simulate neutral pH.

Figure 7a shows snapshots of a 5 ns-long reversible-motion simulation of M3. Increasing the pH back to neutral triggered the reversible transition of the mutant and the final conformation generated by this simulation resembles the

initial starting structure from the closed-to-open simulation (Figure 5b). Figure 7b shows the dynamics of the reversible motion of M3 over the simulation time. As mentioned in the previous section, the 'open' state generated at the end of the close-to-open simulation of M3 at low pH was in a state of dynamic equilibrium. This means that the peptide was in a 'tensed' state wherein the restituting forces due to helices elasticity and the hydrophobic attractions near the C-terminal of the peptide chains balanced the repulsive electrostatic forces of the ionized histidine residues. At neutral pH, the force-generating capability vanished due to histidine neutralization, leading to the restitution of the 'relaxed' state. The reversible transition of the mutant at neutral pH was exactly as hypothesized and verifies the concept of designing a nanotweezer element whose actuation can be modulated by pH.

Physicochemical contributions to the nanotweezer motion in M3

In order to probe the physicochemical contributions to the actuation mechanism, we first examined the closed-to-open
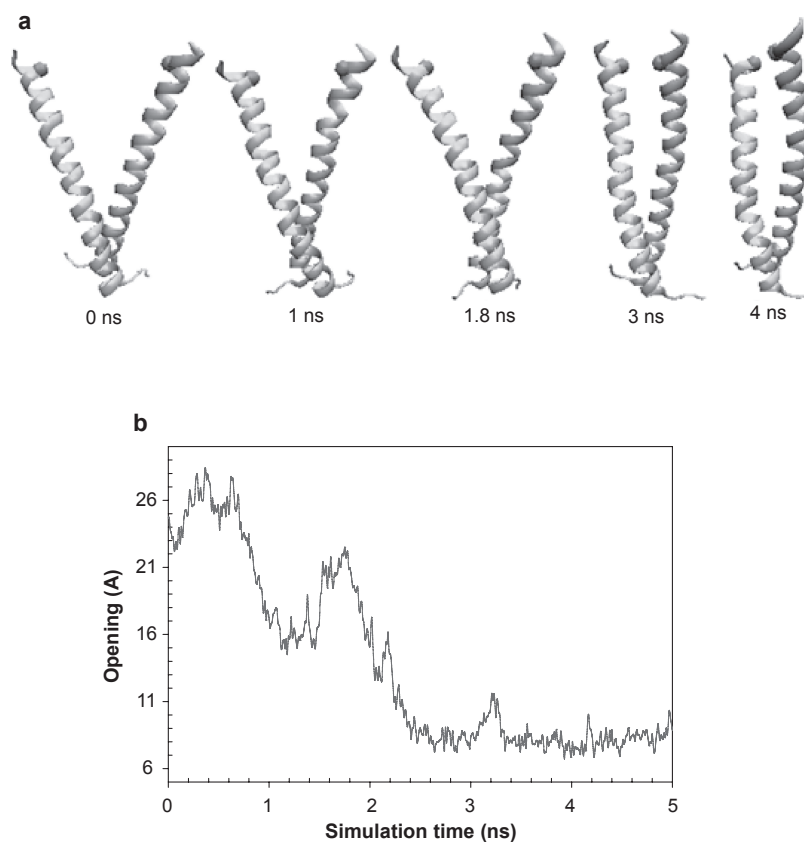

Figure 7 a) Snapshots of a 5 ns simulation of open-to-close transition to show the reversible motion of mutant M3. For reversible motion the His, Glu and Asp residues were unprotonated to simulate neutral pH. Due to lack of ionic repulsions at neutral pH and also due to the attractive hydrophobic interactions the actuator chains rapidly reclosed. The final state closely resembles the initial NMR structure; **b)** Reversible motion dynamics for mutant M3 at neutral pH. The distance between the two chains after 5 ns simulation time was 10 Å which is in good agreement with the separation between the helices in the initial NMR structure.

actuation behavior of M3 at three different pH values: neutral, intermediate, and low. The objective of these simulations was to ascertain if the nanotweezer design based on M3 mutant is sensitive to smaller changes in pH. Figure 8a shows the plots of opening dynamics of M3 at three pH values. As expected, no opening was observed in the mutant at neutral pH due the absence of ionic repulsions in the chains as the His residues are not ionized at neutral pH. The distance between the two helices at the end of closed-to-open simulation at neutral pH is 7 Å which is in good agreement with the distance observed between the helices at the end of the open-to-closed simulation of M3 (Figure 7). At intermediate pH, where the Glu and Asp residues are assumed to be unprotonated and the His residues protonated, the transition closely followed the low pH trajectory until approximately 2.2 ns, at which point the distance between the two chains was 24 Å. From 2.2–3 ns the separation reduced by 4 Å and the two chains finally stabilized at a distance of 20 Å during the last nanosecond. Thus, at intermediate pH the final inter-helical

a

b

Figure 8 a) Opening dynamics of M3 at varying pH. The trajectories plotted at each pH are the average values for two separate MD runs with different initial random seed. The opening at intermediate pH lags that at low pH by 5 Å thereby suggesting the potential use of the nanotweezer as a pH sensor; **b**) Root mean squared deviations (RMSD) of individual residues of the M3 mutant during the opening and closing mechanism. The plot helps to identify the more flexible region of the protein.

opening was 9 Å, in contrast to the separation of 16 Å seen at low pH. Each chain of mutant M3 has five glutamic acids (Glu254, Glu258, Glu268, Glu270, Glu280) and one aspartic acid (Asp255) residue. These residues are negatively charged at intermediate pH and can be expected to contribute to the overall ionic repulsion, resulting in increased separation between the two chains. However, the opening of M3 at intermediate pH was less than that at low pH by 7 Å. One explanation for this reduced opening lies in the location of the Glu and Asp residues along the protein chain. The Asp255 and Glu280 residues are at the *f* and *c* position respectively on the helical wheel diagram (Figure 1c) of the protein. The *f* and *c* positions are at the outer periphery of the protein and thus these residues are not expected to participate in any interhelical ionic interactions. On the other hand, three salt-pairs (Glu268A–Lys263B, Lys275A–Glu270B, Lys275B–Glu270A) contribute to interhelical ionic attractions at the intermediate pH thereby significantly reducing the total ionic repulsions between the two chains resulting in a reduced separation between the chains. These salt-pairs are absent at low pH due to the protonation of Glu residues which permits greater opening between the helices. This qualitative explanation neglects the fact that the Glu, Asp, and His residues are most likely only partially protonated at intermediate pH values, and also neglects possible cooperative effects in the acid-base equilibria of adjacent residues. Nevertheless, these approximations do not alter the overall conclusion that the results at intermediate and low pH support our hypothesis that the opening of the nanotweezer can be modulated simply by varying the pH of its environment.

We next compared the variation of solvent accessible surface area (SASA) of mutant M3 under neutral and low pH conditions. The SASA is calculated by rolling a sphere of solvent (water) molecule with a probe radius of 1.4 Å over the protein (Shrake and Rupley 1973). Changes in the SASA of the residues located in the region between residues His243 and His261 were computed as a function of time (Figure S-4). Under low pH conditions the SASA value increased from 4250 $Å^2$ to approximately 4700 $Å^2$ indicating increasing solvent exposure of buried residues due to pH-induced actuation. The residues near the C-terminus remained protected from the solvent due to the strong hydrophobic binding between the residues in this region of the peptide ('hydrophobic core', see Figure S-2). As expected for a pH change from low to neutral, the SASA value decreased due to the reduction in solvent exposure during the open-to-close transition of the mutant.
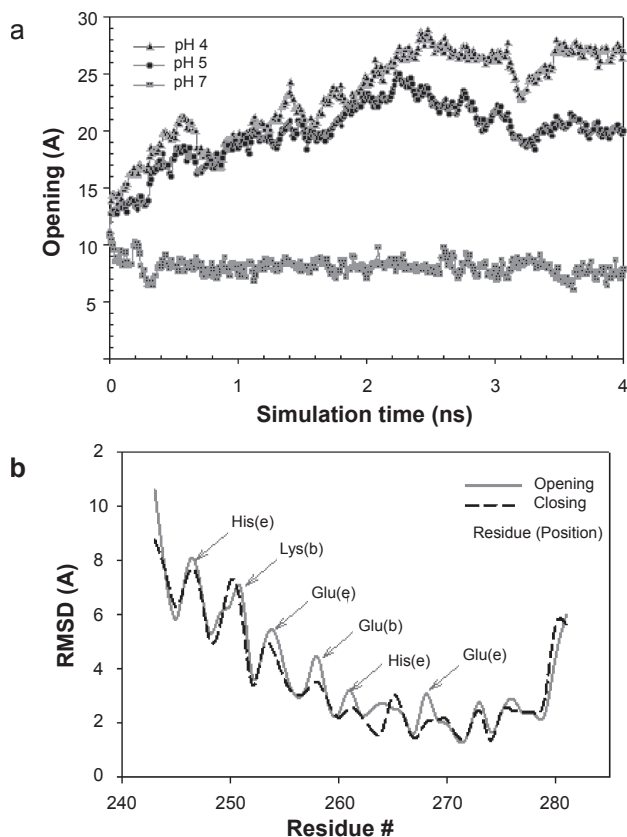
In order to investigate the contributions from individual residues further, we identified the flexible region of the peptide that contributes to the opening dynamics. Figure 8b shows the plot of the total RMSD for each residue during the close-to-open (low pH) and open-to-close (neutral pH) transitions. The region of the peptide lying between residues 243 and 260 is significantly flexible and shows a per-residue RMSD greater than 3 Å. Also, the His261 and His265 residues were not involved in electrostatic interactions in the peptide since the charge-carrying nitrogen atoms are further than the 13.5 Å cut-off set during MD simulations for calculating possible electrostatic interactions. Nevertheless, these mutations play an important part by reducing the hydrophobic binding and increasing the flexibility of the peptide when compared with the parent residues. Residues 262–279 remained strongly associated with significantly low RMSD values due to stabilizing hydrophobic interactions. The higher RMSD value for residues 280 and 281 near the C-terminus is explained by their random coil structure as a consequence of which these residues undergo high thermal fluctuations resulting in increased RMSD values.

Another interesting feature of the per-residue RMSD plot is the periodicity observed in the curve. The periodicity in the RMSD values of the residues follows the same trend during both the *opening* and *closing* mechanism of the nanotweezer. Further investigation revealed that the 'peaks' in the RMSD curve correspond to His247, Lys251, Glu254, Glu258, His261, and Glu268 residues occupying the *e*, *b*, *e*, *b*, *e*, *e* positions respectively along the heptad repeat (see Figure 1c for helical wheel diagram showing the heptad repeat positions). Given that histidine, lysine, and glutamic acids are polar residues and the *e* position in the heptad repeat is involved in electrostatic interactions, it may be surmised that the presence of polar residues in this position plays an important role in the overall flexibility of the peptide.

Modulation of DNA-binding activity

The pH dependent conformational change of the nanotweezer can be employed for modulating the DNA-binding affinity of the parent GCN4 transcription activator protein. The design principle can also be employed to generate proteins with distinct DNA-binding specificities and different physiological targets thereby having implications in engineering of novel transcription factors and ligand design for DNA purification. To demonstrate the DNA-binding modulation capability of the nanotweezer a new peptide was designed in which the DNA-binding basic region of the parent GCN4 peptide was grafted at the end of the N-terminus of the nanotweezer based on the M3 mutant

design (henceforth called GCN4mT). The residue sequence of the resulting GCN4mT peptide is shown in Figure 9a.

Two simulations were carried out to study the GCN4mT–DNA complex at low and neutral pH respectively. It was hypothesized that the conformational opening in the GCN4mT and protonation (and hence neutralization) of charges on the adenosine nucleotides at low pH (Aksimentiev et al 2004) would result in the reduction of the GCN4mT-DNA-binding activity in turn resulting in the release and diffusion of DNA molecule away from the GCN4mT-binding site. However, diffusion is an extremely slow process governed mostly by random Brownian motions and hence is difficult to simulate in typical MD timescales. In order to 'accelerate' the diffusion process and therefore, obtain quantitative data on the strength of GCN4mT–DNA binding, we employed the SMD technique. The DNA molecule was pulled out of the GCN4mT-binding site using a constant velocity SMD simulation and the force required for this pull was computed and plotted. Each simulation was further divided into two runs: In the first run a normal 4-ns MD simulation (without applying SMD) was carried out on the GCN4mT–DNA complex to let the system evolve naturally and change conformation. A second 4-ns long MD simulation was then started from the end point of the first simulation but this time the C-terminal residues of the peptide were held fixed while the DNA atoms were pulled out with a constant velocity.

Figure 9b,c shows the simulation snapshots of the GCN4mT–DNA complex at neutral and low pH values. No major conformational changes were observed in the GCN4mT–DNA system at neutral pH during the first 4 ns of simulation (Figure 9b). This was expected, firstly because at neutral pH there are no electrostatic repulsive forces 'pushing' the peptide chains since the histidine residues are unionized. Secondly, the DNA bases as well as phosphate backbone is negatively charged at neutral pH and hence binds electrostatically with the positively charged residues in the DNA-binding region of the peptide. For the next 4 ns the C-terminal residues (Arg281) in both peptide chains were held fixed and the DNA atoms were pulled with a constant velocity in the direction of the vector joining the center-of-mass (COM) of DNA atoms and the COM of the fixed Arg281 residues in the peptide chains. This effectively pulls out the DNA along the longitudinal axis of the peptide. There was no reduction of the DNA-binding capability of the GCN4mT at neutral pH which is evident from the 4–8 ns simulation snapshots in Figure 9b. The strength of the GCN4mT–DNA binding at neutral pH was
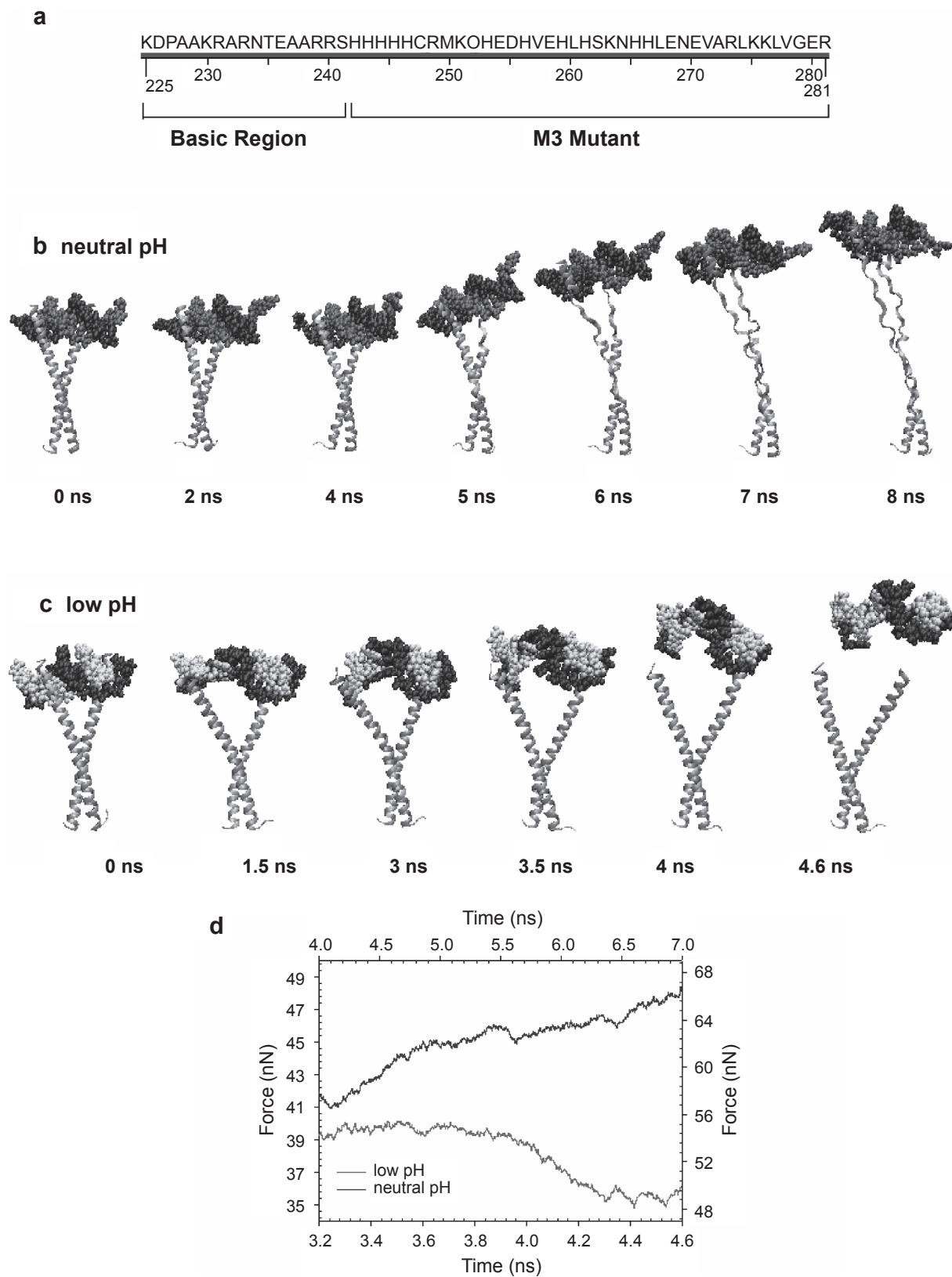
a

KDPAAKRARNTEAARRSHHHHHCRMKOHEDHVEHLHSKNHHLENEVARLKKLVGER

225 230   240   250   260   270   280
                                                      281

Basic Region   **M3 Mutant**

b neutral pH

0 ns   2 ns   4 ns   5 ns   6 ns   7 ns   8 ns

c low pH

0 ns   1.5 ns   3 ns   3.5 ns   4 ns   4.6 ns

d

Figure 9 a) Residue sequence of the GCN4mT peptide. The basic DNA-binding region is grafted at the N-terminus of the mutant M3 design; Snapshots of the SMD simulation to study DNA-binding modulation; **b**) at neutral pH the DNA molecule is tightly bound to the peptide chains and cannot break free when pulled using an external force; **c**) At low pH the conformational changes in the GCN4mT peptide reduces the strength of DNA-binding and when pulled the DNA molecule is rapidly released from the peptide-binding cavity; **d**) Force required pulling the DNA out of the GCN4mT-binding cavity. The Left and Bottom axis are for data at low pH while the Top and Right axis are for neutral pH data. As hypothesized the force required to pull the DNA is considerably smaller at low pH.

such that instead of the DNA molecule being released from the GCN4mT-binding pocket, the force applied on the DNA atoms was transferred to peptide chains and the α-helices started to unfold under its influence.

At low pH, a significant nanotweezer actuation mechanism was observed in the GCN4mT peptide during the initial 4 ns of simulation; the actuation was a result of the electrostatic repulsive forces in the M3 coiled-coil portion. The average RMSD of the Cα atoms was 4.3 Å at low pH which is significantly higher when compared to 2.2 Å RMSD at neutral pH. At low pH, the system was initially simulated till the Cα RMSD for the peptide stabilized at a constant value (4.3 Å) signifying that the peptide had achieved a stable 'open' state. This corresponds to the 3.2 ns mark in the simulation timeline. At this stage the C-terminal residues (Arg281) were fixed and the DNA molecule was 'pulled' using a constant velocity. As can be seen from the simulation snapshots shown in Figure 9c, the DNA molecule was rapidly released from the GCN4mT-binding cavity without destabilizing the protein secondary structure. The force required to pull the DNA was computed using Eq. 1 and plotted. Figure 9d shows the plot of this force at both the neutral and low pH values. The force required to pull the DNA from the GCN4mT-binding cavity is much weaker at low pH then at neutral pH. At low pH a 40 nN force was being applied to the DNA molecule to overcome the peptide-DNA interactions. At the 3.9 ns stage, the DNA molecule started to break free from the peptide which resulted in a weaker 'pulling' force from this point on. At the 4.4 ns stage, the DNA molecule is completely free from the peptide-binding cavity and the only force required is the friction force to drag it through the water box which is signified by the flattening of the force curve at a low (35 nN) value. At neutral pH, however, due to no initial conformational 'opening' in the GCN4mT peptide maintain strong peptide-DNA interactions as indicated by a higher value of force (58 nN) initially being applied on the DNA,. This applied force increases with simulation time due to the additional work is being performed upon unfolding of the coiled-coil α-helices.

Taken together, the SMD simulation results (Figure 9b,c) in conjunction with the force profiles (Figure 9d) suggests a reduced DNA-binding of the GCN4mT peptide at low pH when compared to neutral pH and confirms our hypothesis that DNA-binding activity of the GCN4 peptide can be engineered in order to obtain environmentally-responsive mutants as exemplified by the pH-activated nanotweezer in this case. Environmentally responsive DNA-binding protein systems can lead to practical tools for the studying cellular chemistry and controlling transcription process. Several groups have reported techniques for controlling DNA-binding ability of basic zipper domains and cross-linked peptide constructs with applications in drug delivery either independently (Walensky et al 2004; Futaki 2005) or in conjunction with cell-penetrating peptides (Kawamura et al 2006). Examples of these techniques include the reversible photocontrol of designed GCN4-bZIP proteins using a azobenzene chromophore (Woolley et al 2006) and the design of a negative vitellogenin promoter-binding protein (VBP) leucine zipper (Moll et al 2000). In a similar fashion, we propose that our nanotweezer construct may also have applications in drug delivery; drug-binding domains may be grafted at the N-terminus of the tweezer which can be employed for releasing the bound drug by inducing repulsions in the helices of the coiled-coil upon pH activation.

Conclusions

We have described the design, evolution, and evaluation of a pH-dependent coiled-coil nanotweezer using molecular dynamics simulations. We designed four mutants based on the parent coiled-coil GCN4-LZ protein containing histidine tags (five histidines) and up to five point histidine mutations along the helical chains. One of the mutants, M3, showed optimal performance characteristics while maintaining its structural integrity during the entire operation. Upon pH actuation, M3 opened up to 27 Å, which is a significant displacement considering the initial separation between the two chains was only 11 Å. Importantly, this actuation behavior was reversible upon restoration of initial pH conditions. Our results shed significant light on molecular interactions involved in coiled-coil stability and the role of molecular interactions in incorporating flexibility in rigid peptide motifs. Accommodating protein flexibility has implications in computational drug design wherein one of the goals is to design a receptor that is flexible enough to accommodate multiple binding modes of the same ligand. The ability to incorporate flexibility in protein receptor domains can therefore lead to novel drug design and/or to properly predict the activity of existing inhibitors (Carlson and McCammon 2000). In addition to the observation that electrostatic interactions in a protein motif are sensitive to the location, orientation and neighborhood of electrostatic charges and that these charges can be modified by modulating the pH, our results highlight the utility of computational modeling for protein design and stability analysis. Our preliminary computational results show that engineering of novel transcription factor is a potential application of

the nanotweezer wherein pH-dependent DNA-binding modulation can be achieved by grafting a DNA-binding domain at the N-terminus of the peptide chains.

We have recently experimentally demonstrated the reversible opening and closing of a truncated version of the M1 peptide by electron spin resonance (Gullà SV, pers comm. 2008). Briefly, a sequence with a trihistidine tag and the TOAC (Toniolo et al 1995) amino acid spin label immediately N-terminal to the leucine zipper region was synthesized. The distance between the labels in the dimer measured by double electron-electron resonance (DEER) spectroscopy (Eaton and Eaton 2000) at low and neutral pH. At pH 7, the spin-spin distance exhibits a tight distribution around 23 Å, identical to the distance predicted from the crystal structure of GCN4. At pH 4, a broad distribution around 36 Å is observed, consistent with the predictions of the MD calculations.

Acknowledgements

References

Aksimentiev A, Heng JB, Timp G, et al. 2004. Microscopic kinetics of DNA translocation through synthetic nanopores. *Biophys J*, 87:2086–97.

Aurora R, Srinivasan R, Rose GD. 1994. Rules for alpha-helix termination by glycine. *Science*, 264:1126–30.

Banta S, Megeed Z, Casali M, et al. 2007. Engineering protein and peptide building blocks for nanotechnology. *J Nanosci Nanotechnol*, 7:387–401.

Bao G, Suresh S. 2003. Cell and molecular mechanics of biological. materials. *Nat Mater*, 2:715–25.

Barbara K, Willis K, Haley T, et al. 2007. Coiled coil structures and transcription: an analysis of the S. cerevisiae coilome. *Mol Genet Genomics*, 278:135–47.

Beerli RR, Barbas CF, 3rd. 2002. Engineering polydactyl zinc-finger transcription factors. *Nat Biotechnol*, 20:135–41.

Bella J, Eaton M, Brodsky B, et al. 1994. Crystal and molecular structure of a collagen-like peptide at 1.9 A resolution. *Science*, 266:75–81.

Biju V, Itoh T, Anas A, et al. 2008. Semiconductor quantum dots and metal nanoparticles: syntheses, optical properties, and biological applications. *Anal Bioanal Chem*, 391:2469–95.

Bloom JD, Meyer MM, Meinhold P, et al. 2005. Evolving strategies for enzyme engineering. *Curr Opin Struct Biol*, 15:447–52.

Brannigan JA, Wilkinson AJ. 2002. Protein engineering twenty years on. *Nat Rev Mol Cell Biol*, 3:964–70.

Bustamante C. 2004. Of torques, forces, and protein machines. *Protein Sci*, 13:3061–5.

Carlson HA, McCammon JA. 2000. Accommodating protein flexibility in computational drug design. *Mol Pharmacol*, 57:213–8.

Cheng F, Shen J, Luo X, et al. 2002. Steered molecular dynamics simulations on the "tail helix latch" hypothesis in the gelsolin activation process. *Biophys J*, 83:753–62.

Columbus L, Hubbell WL. 2004. Mapping backbone dynamics in solution with site-directed spin labeling: GCN4-58 bZip free and bound to DNA. *Biochemistry*, 43:7273–87.

Crick FHC. 1953. The packing of α-helices: simple coiled-coils. *Acta Crystallogr*, 6:689–97.

Daggett V, Fersht A. 2003. The present view of the mechanics of protein folding. *Nat Rev Mol Cell Biol*, 4:497–502.

Darden T, York D, Pedersen L. 1993. Particle mesh Ewald. An Nlog(N) method for Ewald sums in large systems. *J Chem Phys*, 98:10089–92.

Doerr AJ, Case MA, Pelczer I, et al. 2004. Design of a functional protein for molecular recognition: specificity of ligand binding in a metal-assembled protein cavity probed by 19f NMR. *J Am Chem Soc*, 126:4192–8.

Eaton SS, Eaton GR. 2000. Distance measurements in biological systems by EPR. New York, NY: Academic/Plenum Pub.

Ellenberger TE, Brandl CJ, Struhl K, et al. 1992. The GCN4 basic region leucine zipper binds DNA as a dimer of uninterrupted alpha helices: crystal structure of the protein-DNA complex. *Cell*, 71:1223–37.

Frishman D, Argos P. 1995. Knowledge-based protein secondary structure assignment. *Proteins*, 23:566–79.

Futaki S. 2005. Membrane-permeable arginine-rich peptides and the translocation mechanisms. *Adv Drug Deliv Rev*, 57:547–58.

Gao M, Craig D, Vogel V, et al. 2002. Identifying unfolding intermediates of FN-III(10) by steered molecular dynamics. *J Mol Biol*, 323:939–50.

Gooding JJ, Chow E, Finlayson R 2003. Biosensors for detecting metal ions: New trends. *Aus J Chem*, 56:159–62.

Harbury PA. 1998. Springs and zippers: coiled coils in SNARE-mediated membrane fusion. *Structure*, 6:1487–91.

Hendsch ZS, Tidor B. 1999. Electrostatic interactions in the GCN4 leucine zipper: substantial contributions arise from intramolecular interactions enhanced on binding. *Protein Sci*, 8:1381–92.

Heng JB, Aksimentiev A, Ho C, et al. 2006. The electromechanics of DNA in a synthetic nanopore. *Biophys J*, 90:1098–106.

Hirsch LR, Gobin AM, Lowery AR, et al. 2006. Metal nanoshells. *Ann Biomed Eng*, 34:15–22.

Isralewitz B, Baudry J, Gullingsrud J, et al. 2001. Steered molecular dynamics investigations of protein function. *J Mol Graph Model*, 19:13–25.

Jorgensen WL, Chandrasekhar J, Madura JD. 1983. Comparison of simple potential functions for simulating liquid water. *J Chem Phys*, 79:926–35.

Karplus M, McCammon JA. 2002. Molecular dynamics simulations of biomolecules. *Nat Struct Biol*, 9:646–52.

Kawamura KS, Sung M, Bolewska-Pedyczak E, et al. 2006. Probing the impact of valency on the routing of arginine-rich peptides into eukaryotic cells. *Biochemistry*, 45:1116–27.

Kohn WD, Kay CM, Hodges RS. 1995. Protein destabilization by electrostatic repulsions in the two-stranded alpha-helical coiled-coil/leucine zipper. *Protein Sci*, 4:237–50.

Lee EH, Gao M, Pinotsis N, et al. 2006. Mechanical strength of the titin Z1Z2-telethonin complex. *Structure*, 14:497–509.

Lu H, Schulten K. 1999. Steered molecular dynamics simulations of force-induced protein domain unfolding. *Proteins*, 35:453–63.

Lu S, Long M. 2005. Forced dissociation of selectin-ligand complexes using steered molecular dynamics simulation. *Mol Cell Biomech*, 2:161–77.

MacKerell AD, Bashford D, Bellott M, et al. 1998. All-atom empirical potential for molecular modeling and dynamics studies of proteins. *J Phys Chem*, 102:3586–616.

Martyna GJ, Tobias DJ, Klein ML. 1994. Constant pressure molecular dynamics algorithms. *J Chem Phys*, 101:4177–89.

Mason JM, Arndt KM. 2004. Coiled coil domains: stability, specificity, and biological implications. *Chembiochem*, 5:170–6.

Missimer JH, Steinmetz MO, Jahnke W, et al. 2005. Molecular-dynamics simulations of C- and N-terminal peptide derivatives of GCN4-p1 in aqueous solution. *Chem Biodivers*, 2:1086–104.

Mizoue LS, Chazin WJ. 2002. Engineering and design of ligand-induced conformational change in proteins. *Curr Opin Struct Biol*, 12:459–63.

Mohanty D, Kolinski A, Skolnick J. 1999. De novo simulations of the folding thermodynamics of the GCN4 leucine zipper. *Biophys J*, 77:54–69.

Moll JR, Olive M, Vinson C. 2000. Attractive interhelical electrostatic interactions in the proline- and acidic-rich region (PAR) leucine zipper subfamily preclude heterodimerization with other basic leucine zipper subfamilies. *J Biol Chem*, 275:34826–32.

Moll JR, Ruvinov SB, Pastan I, et al. 2001. Designed heterodimerizing leucine zippers with a ranger of pIs and stabilities up to 10(−15) M. *Protein Sci*, 10:649–55.

Nikolaev Y, Pervushin K. 2007. NMR spin state exchange spectroscopy reveals equilibrium of two distinct conformations of leucine zipper GCN4 in solution. 129:6461–9.

O'Shea EK, Klemm JD, Kim PS, et al. 1991. X-ray structure of the GCN4 leucine zipper, a two-stranded, parallel coiled coil. *Science*, 254:539–44.

Phillips JC, Braun R, Wang W, et al. 2005. Scalable molecular dynamics with NAMD. *J Comput Chem*, 26:1781–802.

Pineiro A, Villa A, Vagt T, et al. 2005. A molecular dynamics study of the formation, stability, and oligomerization state of two designed coiled coils: possibilities and limitations. *Biophys J*, 89:3701–13.

Saenger W. 1984. Principles of Nucleic Acid Structure. New York, NY: Springer-Verlag.

Seungho C, Sean XS. 2005. The elasticity of alpha-helices. *J Chem Physics*, 122:244912.

Shrake A, Rupley JA. 1973. Environment and exposure to solvent of protein atoms. Lysozyme and insulin. *J Mol Biol*, 79:351–71.

Sun S, Chandler D, Dinner AR, et al. 2003. Elastic energy storage in beta-sheets with application to F1-ATPase. *Eur Biophys J*, 32:676–83.

Suzuki K, Hiroaki H, Kohda D, et al. 1998. An isoleucine zipper peptide forms a native-like triple stranded coiled coil in solution. *Protein Eng*, 11:1051–5.

Tama F, Brooks CL. 2006. Symmetry, form, and shape: guiding principles for robustness in macromolecular machines. *Annu Rev Biophys Biomol Struct*, 35:115–33.

Tenne R. 2006. Inorganic nanotubes and fullerene-like nanoparticles. *Nat Nano*, 1:103–11.

Tinoco IJ, Bustamante C. 2002. The effect of force on thermodynamics and kinetics of single molecule reactions. *Biophys Chem*, 101–102:513–33.

Toniolo C, Valente E, Formaggio F, et al. 1995. Synthesis and conformational studies of peptides containing TOAC, a spin-labelled C alpha, alpha-disubstituted glycine. *J Pept Sci*, 1:45–57.

van Gunsteren WF, Berendsen HJC. 1977. Algorithms for macromolecular dynamics and constraint dynamics. *Mol Phys*, 34:1311–27.

Vieth M, Kolinski A, Brooks CL, 3rd, et al. 1994. Prediction of the folding pathways and structure of the GCN4 leucine zipper. *J Mol Biol*, 237:361–7.

Walensky LD, Kung AL, Escher I, et al. 2004. Activation of apoptosis in vivo by a hydrocarbon-stapled BH3 helix. *Science*, 305:1466–70.

Weis WI, Scheller RH. 1998. Membrane fusion. SNARE the rod, coil the complex. *Nature*, 395:328–9.

Wolf E, Kim PS, Berger B. 1997. MultiCoil: A program for predicting two- and three-stranded coiled coils. *Protein Sci*, 6:1179–89.

Woolley GA, Jaikaran AS, Berezovski M, et al. 2006. Reversible photocontrol of DNA binding by a designed GCN4-bZIP protein. *Biochemistry*, 45:6075–84.

Yu Y, Monera OD, Hodges RS, et al. 1996. Investigation of electrostatic interactions in two-stranded coiled-coils through residue shuffling. *Biophys Chem*, 59:299–314.
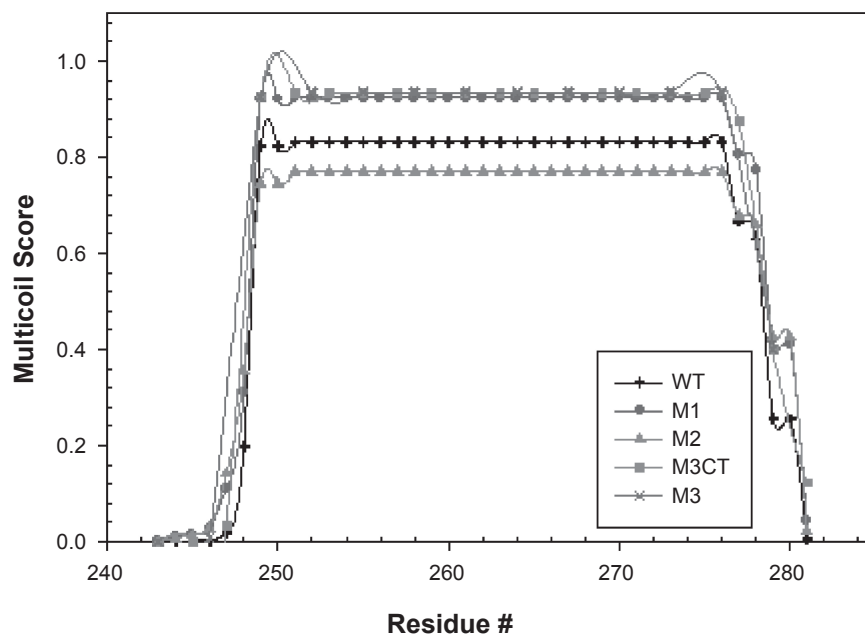
Supporting information

Figure S-1 MultiCoil score for different molecular tweezer mutants. The coiled-coil probability cut-off is 0.5.
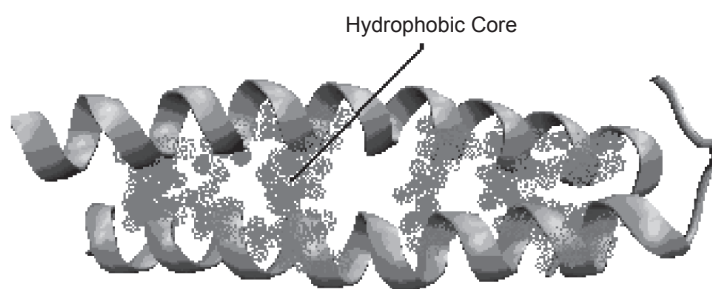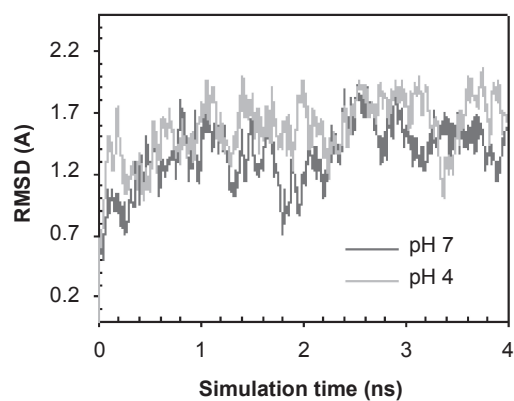

Figure S-2 a) Time dependence of the root mean squared deviation (RMSD), measured with respect to the initial (t = 0) structure of the wild-type (WT) peptide, for all backbone atoms at neutral and low pH. The value agrees well with the reported range of RMSD values from previously MD simulations and also shows that the WT peptide is stable at both low and neutral pH; **b)** Location of the binding hydrophobic cores along the WT structure.
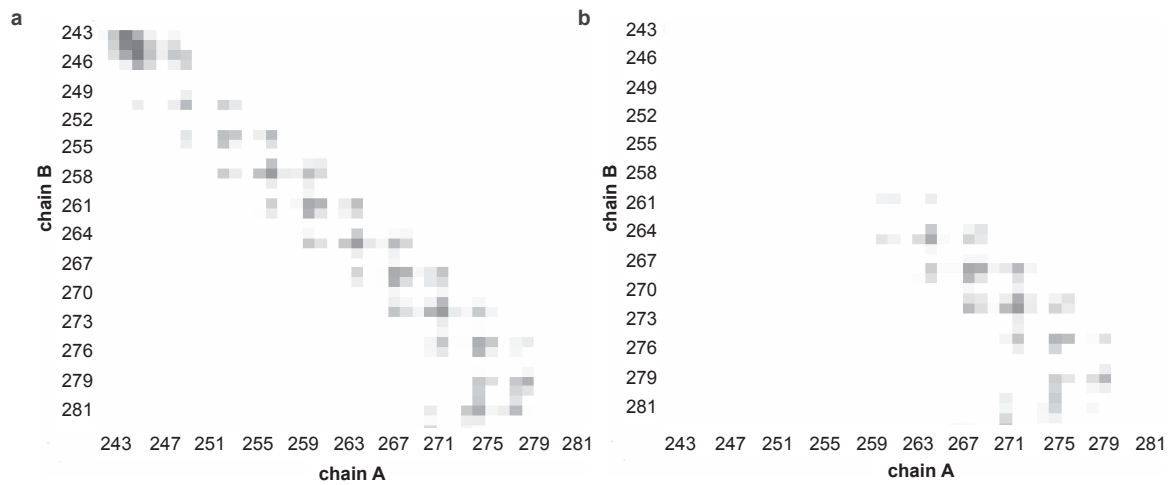
Figure S-3 a) Helix contacts by residue for wild-type GCN4 after 4-ns simulation at low pH; **b**) Helix contacts for mutant M3 after 4-ns simulation at low pH shows that only residues 243–261 in both chains moved during the simulation. The Cα-to-Cα distance for each pair is shown as a square colored by linear grayscale between 0 and 10.0 Å, and white when ≥ 10.0 Å.
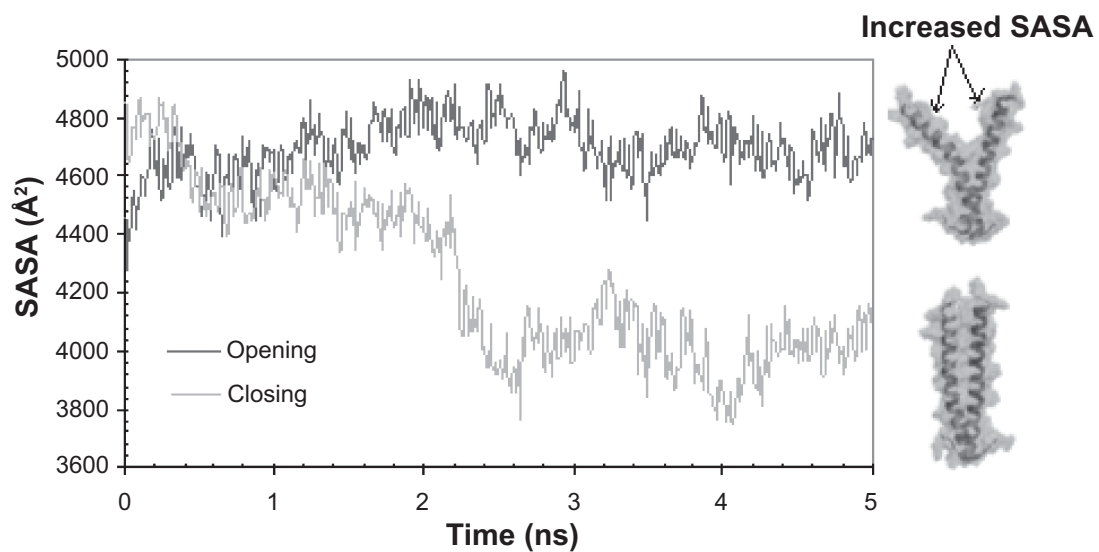

Figure S-4 Solvent accessible surface area (SASA) as a function of time for residues His243 to His261 during the opening and closing mechanism of the nanotweezer. Residues which are initially buried become exposed to the solvent during the opening mechanism. SASA representation of the 'closed' (*Bottom Inset*) state and 'open' state (*Top Inset*) for the nanotweezer showing the increased surface area.